Thiopeptide-Supported Lipid Layers on Solid Substrates

N. Bunjes, E. K. Schmidt, A. Jonczyk, F. Rippmann, D. Beyer, H. Ringsdorf, P. Gräber, W. Knoll, and R. Naumann

Max-Planck-Institut für Polymerforschung, Ackermannweg 10, 55128 Mainz, Germany, Institut für Organische Chemie, Johannes-Gutenberg-Universität Mainz, 55099 Mainz, Germany, Institut für Physikalische Chemie, Albert-Ludwigs-Universität Freiburg, 79104 Freiburg, Germany, and Merck KGaA, 64271 Darmstadt, Germany

Langmuir®
The ACS Journal of Surfaces and Colloids

Reprinted from
Volume 13, Number 23, Pages 6188–6194

Thiopeptide-Supported Lipid Layers on Solid Substrates

N. Bunjes,[†] E. K. Schmidt,[†] A. Jonczyk,[‡] F. Rippmann,[‡] D. Beyer,[§] H. Ringsdorf,[§] P. Gräber,[∥] W. Knoll,*[,†] and R. Naumann[‡]

Max-Planck-Institut für Polymerforschung, Ackermannweg 10, 55128 Mainz, Germany, Institut für Organische Chemie, Johannes-Gutenberg-Universität Mainz, 55099 Mainz, Germany, Institut für Physikalische Chemie, Albert-Ludwigs-Universität Freiburg, 79104 Freiburg, Germany, and Merck KGaA, 64271 Darmstadt, Germany

Received March 26, 1997. In Final Form: August 5, 1997[⊗]

The sequential layer-by-layer formation of peptide-supported bimolecular lipid membranes at solid supports is described. In the first step, thiol-derivatized peptide sequences of 5 and 7 amino acids are assembled on a Au substrate. After activation of their COOH-terminus phospholipid molecules (DMPE) are covalently attached via an amid bond to form a tethered monolayer on the Au electrode. The different preparation steps are analyzed by Fourier transform IR, X-ray reflectometry, and surface plasmon spectroscopy. The latter technique is then also used to on-line monitor at the solid/solution interface the formation of a bilayer by fusion of vesicles prepared from a fluid lipid mixture with and without reconstituted proteins. The obtained thicknesses and capacitance values are compatible with the tethered bilayer model and point to an incorporation of ATPase into these membrane matrices.

1. Introduction

Solid-supported lipid layers are considered as model sytems for biological membranes.[1,2] They are designed to incorporate membrane proteins only if a spacer group separates the lipid layer from the support. The purpose of such a spacer is to provide an aqueous layer to accommodate hydrophilic domains of the protein and to render transport possible from one side of the lipid phase to the other. Poly(oxyethylene)[4] and other polymer spacer groups[5−10] were employed for this purpose as well as short hydrophilic spacers. Another approach is to design a spacer of defined length and composition having a more rigid structure such as a peptide. Such peptides were first introduced by Rothe and Aurich[11,12] on top of polyacrylic beads. These peptides were then lipid-functionalized in situ to form lipid mono- and bilayers. Bacteriorhodopsin incorporated into these layers was shown to transport protons.[12] In a preliminary report[13] we introduced sulfur-functionalized peptides designed to attach to gold surfaces. Because of their low solubility these peptides were functionalized by a lipid (DMPE) in situ rather than in the bulk to form a peptide-supported lipid monolayer. After fusion with liposomes these monolayers spontaneously formed lipid bilayers designed to incorporate H^+−ATPase from chloroplasts and *E. coli* whose activity was being preserved.[14] This model system will be investigated in the present paper with respect to the arrangement and order of these membrane architectures following the different stages of preparation. Furthermore, the fusion process of liposomes with the lipid monolayers to form lipid bilayers will be investigated, particularly with respect to accumulation and exchange of membrane spanning proteins such as the H^+−ATPase.

2. Materials and Methods

2.1. Materials. 2.1.1. Preparation of the Thiopeptides. Lip-$(Ala)_5$-COOH (lip = lipoic acid) (I) and HS-$(CH_2)_2$-CO-Ala-Ser-Ser-Ala-Ala-Ser-Ala-COOH (II) were obtained by solid phase peptide synthesis in a continuous flow synthesiser[15] using Fmoc (9-fluorenylmethoxycarbonyl) strategy[16] with acid labile side chain protection on an acid labile Wang resin. Washes were done with DMA ((dimethylamino)acetamide), cleavage of the Fmoc-protection group was achieved with 20% piperidin in DMF (dimethylaminoformamide). Triple couplings of 1.3 equiv each with DIC/HOBt (diisopropylcarbodiimide/*N*-hydroxobenzotriazole) for 20 min were followed by capping with Ac_2O/pyridine/DMF 2/3/15 (vol.) for 10 min. The synthesis was monitored continuously by UV spectroscopy at 310 nm. Loading of the starting amino acid and peptide bound to the resin was quantified by Fmoc-determination.[16] After removal of the Fmoc groups the peptide on the resin was modified at the N-terminus with tritylmercaptopropionic acid or lipoic acid using the normal coupling procedure. Tritylmercaptopropionic acid has been obtained by tritylation of mercatopropionic acid in dichloromethane with excess of triphenylmethanol and TFA (trifluoracetic acid) catalysis at room temperature. The peptide (DE 4444893 41) was removed from the resin and its side chain protection groups were cleaved by treatment with TFA/CH_2Cl_2/anisol 60/40/1 (20 mL/g of resin) for 2−4 h at room temperature. To remove trityl functions TFA/CH_2Cl_2/thiophenol 70/20/10 was used instead. The filtrate was concentrated and the peptide precipitated with ether. Purification was achieved by gel filtration in 2-propanol/water 80/20 with 0.05% TFA on Sephadex G10 and HPLC on Lichrosorb RP 8 in 0.3% TFA with a gradient

[†] Max-Planck-Institut für Polymerforschung.
[‡] Merck KGaA.
[§] Johannes-Gutenberg-Universität Mainz.
[∥] Albert-Ludwigs-Universität Freiburg.
[⊗] Abstract published in *Advance ACS Abstracts,* September 15, 1997.

(1) Ulman, A. *An Introduction to Ultrathin Organic Films: From Langmuir Blodgett to Self-Assembly*; Academic Press, Boston: MA, 1991.
(2) Sackmann, E. *Science* **1996**, *271*, 43.
(3) Lang, H.; Duschl, C.; Vogel, H. *Langmuir* **1994**, *10*, 197.
(4) Duschl, C.; Liley, M.; Lang, H.; Ghandi, A.; Zakeeruddin, S. M.; Stahlberg, H.; Dubochet, J.; Nemetz, A.; Knoll, W.; Vogel, H. *Mater. Sci. Eng.* **1996**, *C 4*, 7−18.
(5) Spinke, J.; Yang, J.; Wolf, H.; Liley, M.; Ringsdorf, H.; Knoll, W. *Biophys. J.* **1992**, *63*, 1667.
(6) Erdelen, C.; Häussling, L.; Naumann, R.; Ringsdorf, H.; Wolf, H.; Yang, J.; Liley, M.; Spinke, J.; Knoll, W. *Langmuir* **1994**, *10*, 1246.
(7) Kuhl, T. L.; Leckband, D. E.; Lasic, D. D.; Israelachvilli, J. N. *Biophys. J.* **1994**, *66*, 1474.
(8) Needham, D.; McIntosh, T.; Lasic, D. D. *Biochim. Biophys. Acta* **1992**, *1108*, 40.
(9) Wegner, G. *Thin Solid Films* **1992**, *216*, 105.
(10) Elender, G.; Kühner, M.; Sackmann, E. *Biosens. Bioelectron.* **1996**, *11*, 565−577.
(11) Rothe, U.; Aurich, H. *Biotechnol. Appl. Biochem.* **1989**, *11*, 18.
(12) Rothe, U.; Aurich, H.; Engelhardt, H.; Oesterhelt, D. *FEBS Lett.* **1990**, *263*, 308.
(13) Naumann, R.; Jonczyk, A.; Kopp, R.; van Esch, J.; Ringsdorf, H.; Knoll, W. Gräber, P. *Angew. Chem.* **1995**, *34*, 2056.
(14) Naumann, R.; Jonczyk, A.; Hampel, C.; Ringsdorf, H.; Knoll, W.; Bunjes, N.; Gräber, P. *Bioelectrochem. Bioenerg.* **1997**, *42*, 241.
(15) Jonczyk, A.; Meienhofer, J. In *Peptides Proc. 8th Am. Pept. Symp.*; Hruby, V., Rich, D. H., Eds.; PierceCo., 1983; pp 73−77.
(16) Chang, C. D.; et al. *Int. J. Pept. Prot. Res.* **1980**, *15*, 485.

S0743-7463(97)00317-X CCC: $14.00

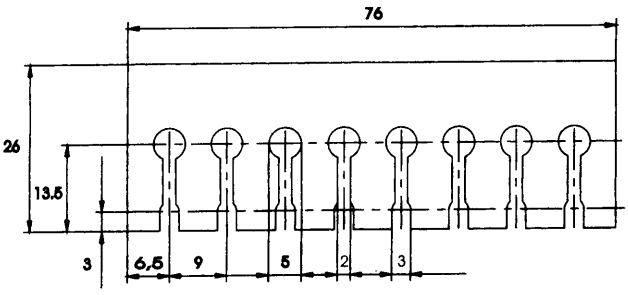

Figure 1. Pattern of eight gold electrodes obtained by electrothermal evaporation on top of glass slides.

of 0–80% 2-propanol. Purity of the peptides was determined by high-performance liquid chromatoraphy (HPLC) to be usually better than 95,% and identity has been found as expected by FAB-MS (fast atom bombardment mass spectroscopy).

2.1.2. Preparation of the Thiopeptide–Lipid Monolayers. The gold substrates were incubated in a solution of the thiopeptide in TFA (1 mg mL^{-1}) for 96 h. After rinsing with TFA, DMF and CH_2Cl_2 slides were placed in a solution of 1 mg mL^{-1} DMPE (dimyristoylphosphatidylethanolamine) in a mixture of DMF, CH_2Cl_2, and LiCl 20/40/0.4 (v/v/w) and the terminal COOH groups of the peptide were activated with 20 μL mL^{-1} DIC (diisopropyl carbodiimide) and coupled by incubation for a further 96 h after adding 10 μL mL^{-1} *N*-ethyldiisopropylamine. Activation and coupling were once more repeated using a fresh coupling mixture. The substrates were then rinsed with DMF and CH_2Cl_2 and dried in a stream of nitrogen. For electrochemical measurements, slides were cut into single electrodes only after forming the lipid monolayers. DMPE and DIC were purchased from Sigma. All other chemicals were Merck reagent grade.

2.1.3. Preparation of the Thiopeptide–Lipid Bilayer. Liposomes were prepared by dialysis[17,18] from phophatidylcholine prepared from eggs (Lipoid E PC) and cholesterol (30%) where indicated. ATPase CF_0F_1 of chloroplasts and EF_0F_1 from *E. coli* was reconstituted into these liposomes using the same procedure. The concentration of the lipid was 8 mg mL^{-1}, while the protein concentration varied from 23 to 461 μg mL^{-1} CF_0CF_1, thus varying the average number of enzymes incorporated corresponding to 1, 10, and 20 CF_0F_1 per liposome, respectively. The average diameter of the vesicles was 150 nm. They are expected to be large unilamellar vesicles (LUVs), i.e., equilibrated with respect to osmotic pressure.

Substrates with the lipid monolayers were incubated at 30 °C overnight if not otherwise indicated in suspensions of these liposomes. Subsequently substrates were rinsed or placed in fresh buffer solution K_2SO_4 0.1 mol L^{-1}, tricine 0.0005 mol L^{-1}, Na_2HPO_4 0.0005 mol L^{-1}, $MgSO_4$ 0.0002 mol L^{-1}, pH = 7.4, sterilized by filtration.

2.1.4. Gold Substrates Used for SPS (Surface Plasmon Resonance Spectroscopy) and XR (X-ray Reflectometry). In order to obtain a good sensitivity for the subsequent XR measurements, the roughness of the glass substrates was minimized. Gold was deposited directly on high refractive index glass LaSFN9 (Berliner Glas) substrates (2.5 × 4 × 0.2 cm^3) by electrothermal evaporation to a thickness of 46 nm for comparison with SPS measurements, after rinsing with ethanol and a mixture of 50% ethanol/toluene. The roughness (root mean square) of the gold films thus obtained was <1 nm.

2.1.5. Gold Substrates Used for Electrochemical and FTIR Measurements. ELKA microscope glass slides (76 × 22 mm^2) were submersed in H_2SO_4 (97%): H_2O_2 (30%) = 7:3 for 2 h, rinsed thoroughly in water from a Millipore still, and dried in an oven at 130 °C. Subsequently gold was deposited to a layer thickness of 60 nm over a sublayer of 5 nm of chromium either covering the whole surface (FTIR) or in a spoonlike pattern (Figure 1) to form eight electrodes per slide. Chromium and gold were deposited by electrothermal evaporation using a Leybold-Heraeus L 650 vapor deposition apparatus at 300 °C and a pressure of 10^{-5}–10^{-6} mbar. Gold substrates were rinsed thoroughly with water and subsequently with methanol and dried in a stream of nitrogen.

(17) Schmidt, G.; Gräber, P. *Biochim. Biophys. Acta* **1985**, *808*, 46.
(18) Schmidt, G.; Gräber, P. *Z. Naturforsch.* **1987**, *42c*, 231.

2.2. Methods. 2.2.1. FTIR Spectroscopy. All FTIR spectra were measured using a Nicolet 5DXC, equipped with an "Ever-Glo" light source and a nitrogen-cooled HgCdTe narrow-band detector. The samples were measured in the dry state in an atmosphere of Ar using a grazing incidence (80°) reflection on an FT80 setup. The spectra were taken with 2500 scans at 4 cm^{-1} resolution and a Happ-Genzel apodization. Temperature for FTIR measurements was always $T = 22 \pm 1$ °C.

2.2.2. X-ray Reflectometry (XR). An 18 kW rotating anode with a graphite monochromator was used working at a wavelength of $\lambda = 1.54$ Å. Reflectivities down to approximately 10^{-6} could be measured. Details on the reflectometer and its performance were reported elsewhere.[19] The sample preparation on Au-coated glass slides (2.5 × 4.0 × 0.2 cm^3) for the reflectivity measurements was identical to that of the following surface plasmon measurements.

The reflected intensities were recorded every 0.004° from θ = 0.1° to 2.0°, measured relative to the sample plane thus covering, in particular, the angular range of the total internal reflection. Generally, one observes in the region of total reflection above the critical angle ($\theta_{crit.}$ = 0.57°), a q^{-4} decrease in the reflected intensity modulated by so-called Kiessig fringes, which are due to the interference of the reflected beams from the various interfaces. The analysis of the reflectivity curves was done by the use of a matrix formalism. All X-ray data were taken at room temperature.

2.2.3. Surface Plasmon Resonance Spectroscopy (SPS). Plasmon surface polaritons (surface plasmons for short) are excited along the metal–dielectric interface. Their field amplitudes decay exponentially, both along the interface and into the dielectricum, with the maximum intensity being at the interface. For an ideal flat surface, the dispersion relation of PSP is given by

$$k_x = \frac{\omega}{c}\sqrt{\frac{\epsilon_m \epsilon_d}{\epsilon_m + \epsilon_d}} \tag{1}$$

with k_x being the surface plasmon wave vector, ω is its frequency, c is the speed of light, $\epsilon_m(\omega) = \epsilon'_m(\omega) + i\,\epsilon''_m(\omega)$ is the complex dielectric function of the metal, and $\epsilon_d(\omega) = \epsilon'_d(\omega) + i\,\epsilon''_d(\omega)$ is the complex dielectric function of the dielectricum. As photons of a laser (HeNe, λ = 632.8 nm) cannot excite surface plasmons directly because their momentum

$$k_x = \frac{\omega}{c}\sin\theta_0 \tag{2}$$

is too small for resonant coupling, a Kretschmann[20] setup is used. For this configuration the refractive index of the prism n_p and the angle of incidence θ_0 define the x-component of the momentum of the exciting photon, where

$$k_x = k_{ph}{}^x = n_p \frac{\omega}{c}\sin\theta_0 \tag{3}$$

In the SPS experiment the angle of incidence is varied and the reflected intensity is detected by a photodiode. A thin dielectric coating of the metal film, e.g., a supported membrane shifts the angle of resonant coupling to surface plasmon modes to higher angles. This angular shift $\Delta\theta$ depends on the thickness d of the layer and its optical properties relative to the surrounding medium, i.e., on the difference between their respective indices of refraction

$$\Delta\theta \sim d(n_1 - n_0) \tag{4}$$

If SPS measurements are performed with the same film (i.e., same d and n_1) but in media of different refractive indices $n_{0,i}$ a separate determination of the layer thickness and its refractive index based on Fresnel calculations is possible.

(19) Foster, M.; Stamm, M.; Reiter, G.; Hüttenbach, S. *Vacuum* **1990**, *41*, 1441.
(20) Raether, H. In *Physics of Thin Films*; Haas, G., Francombe, M. H., Hoffmann, R. W., Eds.; Academic Press: New York, 1977; Vol. 9, p 145.

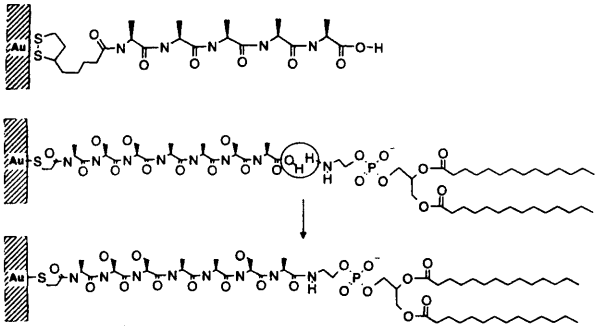

Figure 2. Schematic representation of the thiopeptide monolayer chemisorbed on the gold support and the in situ coupling of terminal COOH groups with DMPE.

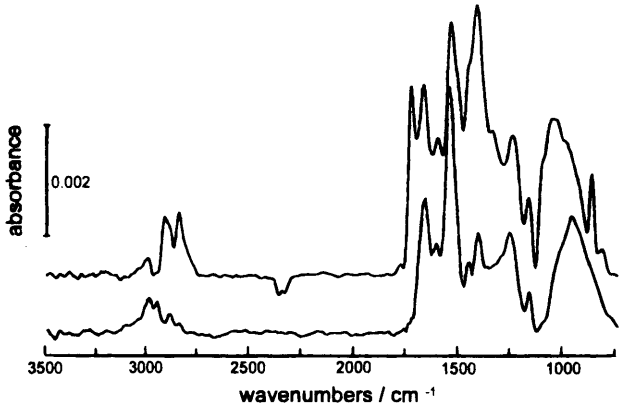

Figure 3. Grazing incidence reflection FT-IR spectra of thiopeptide (lower trace) and thiopeptide-lipid monolayer (upper trace) from 500 to 3500 cm^{-1}, respectively.

Unless otherwise indicated all SPS investigations were done at $T = 30$ °C with the lipid layers being in a fluid state.

2.2.4. Cyclic Voltammetry (CV). Measurements were carried out at 30 °C in the buffer solution given above, in a cell equipped with a silver rod as counter electrode and an Ag/AgCl, saturated KCl as reference electrode using an Autolab instrument (ECO Chemie) and GPES3 software. Potential scan rate and range of potentials were 0.1 V s^{-1} and 0.3 to −0.2 V, respectively.

3. Results

3.1. Characterization of the Thiopeptide and Thiopeptide–Lipid Monolayers. The sequence of preparation steps to form the monolayers on gold substrates is sketched in Figure 2. The thiopeptide is chemisorbed on the gold support via the SH groups thus extending the terminal COOH groups to the outside. The peptide spacer penta-(Ala) introduced by Rothe and Aurich[11,12] is not particularly hydrophilic and is, therefore, replaced by a peptide containing several serines and having terminal SH and COOH groups. After activation in situ, the COOH groups are covalently linked to DMPE to form the thiopeptide-tethered lipid monolayer. These preparation steps are analyzed by the following techniqes

3.1.1. Analysis by FTIR Spectroscopy. The FTIR spectra in Figure 3 show the peptide monolayer chemisorbed on the gold substrate before (lower spectrum) and after the reaction with the lipid DMPE (upper spectrum). For the unreacted peptide monolayer the amide I + II bands at 1644 and 1545 cm^{-1} are observed, as well as several bands of low intensity at 2985, 2946, and 2838 cm^{-1}, which are due to the methyl- and methylene groups of the peptide.

After the reaction of DMPE with the surface bound peptide monolayer additional peaks are found at 1410 and 1730 cm^{-1} which can be attributed to the phosphate and ester functionalities of the lipid, respectively. Furthermore in the alkyl region of the spectrum two bands with increased intensity at 2891 and 2840 cm^{-1} can be observed, which are due to the methylene units of the lipid DMPE. The peak at 1730 cm^{-1} indicates methylene units of a chain length larger than seven ($-CH_2-$).

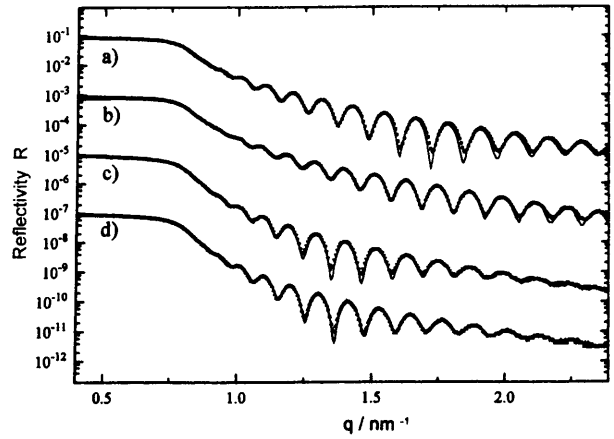

Figure 4. XR spectra of the thiopeptide (b) and the thiopeptide–lipid monolayer after the first (c) and second (d) coupling with DMPE together with that of the bare gold as reference (a). Symbols are experimental data, the full curves are Fresnel calculations with parameters given in Table 1.

3.1.2. Analysis by X-ray Reflectometry. Figure 4 displays a sequence of X-ray reflectometry scans following the same preparation steps. Trace a was taken from the Au-coated glass slide as a reference. A series of Kiessig fringes is observed above the critical angle for total internal reflection at about $q = 0.8$ nm^{-1}, with a characteristic amplitude modulation. The reflection edge is smeared out due to the high absorption coefficient of the Au. The interference pattern originates from the superposition of partial waves reflected at the glass/metal and at the metal/air interface, respectively, and can be modeled by the appropriate Fresnel treatment (full line in Figure 4a). Slight deviations from the experimental data in certain q-ranges are due to minor thickness variations which are averaged slightly different as the angle of incidence varies. This occurs because the footprint size of the X-ray beam on the sample surface is strongly angle dependent. The substrate parameters obtained from this fit calculation, the layer thickness, its electron scattering density $a\rho$ (a = classical electron radius) and two roughness parameters, one characterizing the glass/metal and the other the metal/air interface, are summarized in Table 1.

After chemisorptiom of the thiopeptide to the Au surface the X-ray reflectivity scan shows a characteristic difference (Figure 4, trace b): the angular positions of the Kiessig fringes are shifted and the intensity modulation pattern has slightly changed. Both features can be described by a Fresnel calculation modeling the organic layer with a thickness of 1.5 nm and an electron scattering density given in Table 1. Remarkable is the smooth interface peptide/air characterized by a roughness parameter as low as $\sigma = 0.4$ nm.

The in situ coupling of DMPE to the peptide results in an additional shift of the Kiessig fringes observed in trace c after the first coupling procedure and trace d after the second coupling of Figure 4 together with a pronounced change of the intensity modulation indicating an additional layer. Its mean thickness increment is modeled with $d = 2$ nm, following the second coupling process. The good agreement with experimental data could only be obtained by introducing a significant roughness at the lipid/air interface, as shown in Table 1. This should be taken as a hint as to a not perfectly homogeneous coverage

Table 1. X-ray Reflectivity Data on Glass (LaSFN9) As Obtained from the Analysis Presented in Figure 4[a]

sample	$\sigma_{glass/Au}$ (nm)	d_{Au} (nm)	$\sigma_{Au/air}$ (nm)	$d_{Peptide}$ (nm)	$\sigma_{peptide/air}$ (nm)	d_{Lipid} (nm)	$\sigma_{Lipid/air}$ (nm)
air/Au	0.5	4.6	0.8				
air/peptide/Au	0.5	4.6		1.5	0.4		
air/lipid I monolayer/peptide/Au[b]	0.5	4.6		1.5		1.4	0.7
air/lipid II monolayer/peptide/Au[c]	0.5	4.6		1.5		2.0	0.7

[a] The derived parameters are the interfacial roughness (rms) $\sigma_{i,j}$ between medium i and medium j; the layer thickness d, as well as the following electron scattering density $a\rho$ ($a = 2.8 \times 10^{-13}$ cm). Electron scattering densities: $a\rho_{Au}$ 131.5×10^{10} cm^{-2}, $a\rho_{LaSFN9} = 19.9 \times 10^{10}$ cm^{-2}, $a\rho_{Thiopeptide} = 10.4 \times 10^{10}$ cm^{-2}, $a\rho_{Lipid} = 10.8 \times 10^{10}$ cm^{-2}. [b] After the first lipid-coupling. [c] After the second coupling procedure.

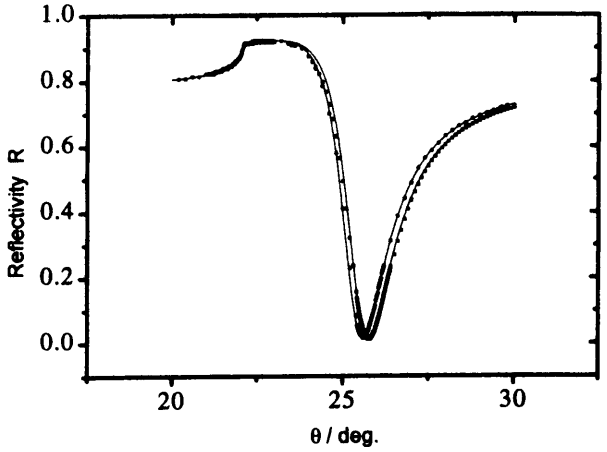

Figure 5. ATR (angular reflectivity) scans in air of the gold substrate as a reference (●) and the thiopeptide monolayer (□).

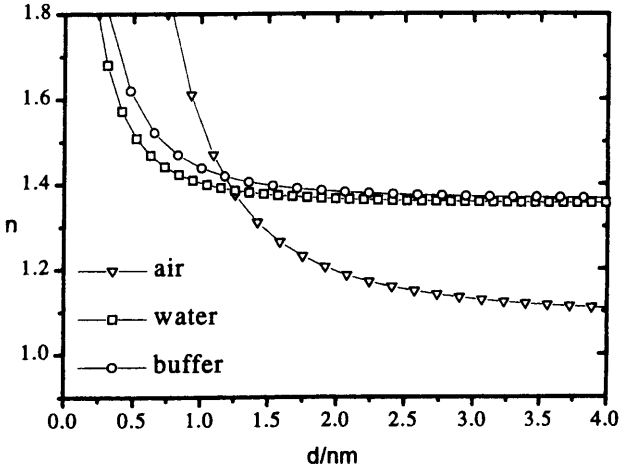

Figure 6. Plot of refractive index n and thickness d pairs obtained in air, water, and buffer (as indicated) according to the Fresnel fit of ATR scans such as the ones displayed in Figure 5 from thiopeptide monolayers.

on the level of the lipid rather than the peptide while the difference between the first and second in situ coupling can be recognized.

3.1.3. Analysis by Surface Plasmon Resonance Spectroscopy (SPS). Figure 5 shows the attenuated total reflectance (ATR) angular reflectivity scans of the thiopeptide monolayer in air together with the scan of the bare gold support as a reference,. Angular shifts of the resonance angle of $\Delta\theta_1 \approx 0.3°$, demonstrate the formation of the peptide layer. In buffer solution, the resonance angles for surface plasmon excitation are higher and the difference between the samples and the reference is smaller. This is due to the higher refractive index of the aqueous solution and hence the lower contrast. Both situations can be well described by the corresponding Fresnel calculations. We have taken ATR reflectivity scans in air, water, and buffer and analyzed according to the Fresnel equation: As outlined in the Experimental Section a plot of all pairs of values (n,d) which are used in the calculation to model the film thickness, d, and its refractive index, n, which are compatible with the three measured angular shifts, $\Delta\theta_i$, should result in a unique separation of n and d. That means all plots obtained from measurements in different bulk media should meet in one crossing point. As seen in Figure 6, the method is not particularly precise because of the crossing area obtained rather than a crossing point. But it gives a certain limited range of thicknesses and refractive indices which are compatible with the optical measurements.

It is interesting to note that the measurement in air is not so sensitive to the refractive index but allows for a fairly accurate thickness determination, whereas the measurement in the aqueous environment largely fixes the refractive index because of the reduced contrast. From the crossing points (or, more precisely, the crossing area) we determine the peptide layer thickness as $d = 1.2$ nm (Table 2), which is remarkably close to the value determined by the X-ray analysis; see below. The obtained

Table 2. Thickness d Measured by SPS of Thiopeptide-Supported Lipid Mono- and Bilayers on Gold, Compared to Lateral Dimensions of The Molecules According to Molecular Modeling Calculations[a]

sample	d (nm)	$d_{theoretical}$ (nm)
peptide	1.2 ± 1	1.6
lipid monolayer/peptide	2.7 ± 4	4.2
lipid bilayer/peptide	5.1 ± 3	
lipid bilayer/peptide with cholesterol 30%	5.6	
lipid bilayer/peptide with 1 ATPase per liposome	8.1	
lipid bilayer/peptide with 10 ATPase per liposome	8.8	
lipid bilayer/peptide with 20 ATPase per liposome	7.3	

[a] Optical parameters: Au, $d = 49.3$ nm, $\epsilon' = -12.657$, $\epsilon'' = 1.461$; peptide, $n = 1.41$; lipid, $n = 1.5$.

refractive index, $n = 1.41$, is sufficiently close to the generally assumed values for proteins ($n = 1.45$). Both values were kept constant in all further Fresnel calculations describing the interfacial architectures with additional lipid layers.

After coupling of the peptide monolayer with DMPE according to Figure 2 the same procedure was applied. The successful covalent binding of DMPE is indicated by an additional angular shift of the plasmon resonance angle in buffer, water, and air (not shown). From an evaluation of these data according to the procedure given above (Figure 6) the refractive index of the lipid layer was deduced to be $n = 1.5$ with the thickness increment being only $d = 1.4$ nm after the second coupling. Compared to the theoretical expectation for the thickness of a lipid monolayer of 2.0−2.5 nm and bearing in mind that the SPS method yields a laterally averaged thickness only, the reduced value points to a partial coverage at the level of the lipid in agreement with the data obtained by X-ray

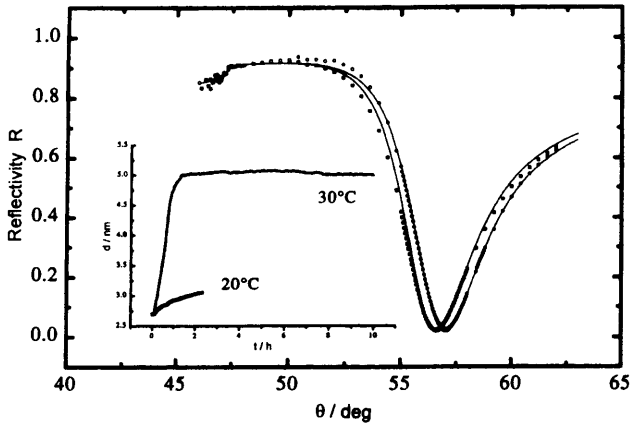

Figure 7. ATR scans of a thiopeptide–lipid monolayer before (□) and after (○) fusion with pure liposomes. Real time recordings at 30 and 20 °C (reflectivity vs time at a constant angle $\theta = 57.5°$) of the fusion process are shown in the insert.

Table 3. Capacitance Values and Peak Separation Measured by Cyclic Voltammetry

sample	capacitance ($F\ cm^{-2}$)	peak separation (mV)
Au	18	
lipid monolayer/peptide/Au	3–5	400
lipid bilayer/peptide/Au	2–3	>600
lipid bilayer/peptide/Au with cholesterol 30%	2–3	>600
lipid bilayer/peptide/Au with ATPase CF_0F_1	2–3	>600

reflectometry. Further qualitative evidence for some monolayer patches on the peptide layer came from reflection–interference microscopic images that clearly showed the lateral optical heterogeneity of the sample, roughly compatible with an ca. 70% coverage by a lipid monolayer.

3.2. Characterization of the Thiopeptide–Lipid Bilayers. In the preliminary report[13] the covalently tethered lipid monolayers had been shown to form lipid bilayers when they are exposed to a suspension of liposomes. Since this occurs in an aqueous environment, the method of choice to follow this process besides electrochemistry[14] is SPS.

3.2.1. Characterization by Cyclic Voltammetry. Table 3 summarizes the data obtained by cyclic voltammetry (CV). The capacitance (C/F) from currents measured by CV in pure buffer solution is calculated[21] according to eq 5

$$C = I/2\nu A \qquad (5)$$

where ν is the voltage scan rate ($V\ s^{-1}$) and A the area of the electrode (cm^2). The factor 2 in the denominator is due to the current I (A) taken as the sum of the numerical cathodic and anodic currents.

So-called peak separations (difference between anodic and cathodic peaks of a reversible redox pair such as cyanoferrate) are taken from voltammograms of this compound at a concentration of 10^{-3} mol/L in the absence and presence of the lipid layers. The peak separation is expectated to be 60 mV at the bare gold electrode getting wider when a dielectric layer covers the gold surface thus preventing diffusion of the redox pair.[22]

(21) Digby, D. Mcdonald *Transient Techniques in Electrochemistry*; Plenum Press: New York and London, 1977.
(22) Sabatini, I.; Rubinstein, J. *J. Phys. Chem.* **1987**, *91*, 6663–6669.

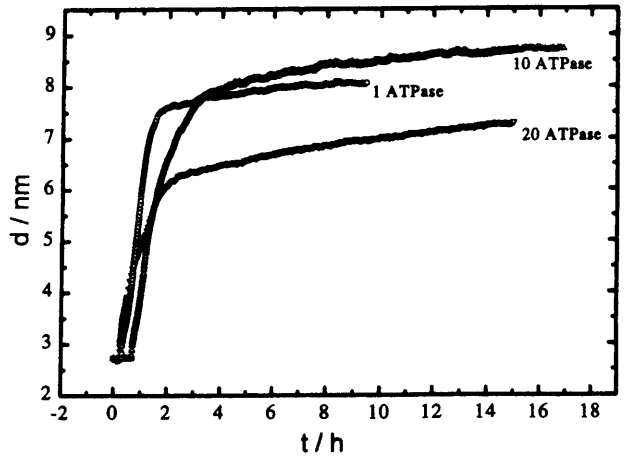

Figure 8. Real time recordings (reflectivity vs time) of the fusion of the thiopeptide–lipid monolayer with liposomes with incorporated ATPase CF_0F_1 the concentration of which with respect to the lipid was 8 mg mL^{-1}, while the protein concentration varied from 23 to 461 $\mu g\ mL^{-1}$ CF_0CF_1 corresponding to an average number of enzymes of 1, 10, and 20 CF_0F_1 per liposome, respectively.

3.2.2. Characterization by Surface Plasmon Resonance Spectroscopy (SPS). Angular ATR scans have been shown above to reflect the average thicknesses of gold and dielectric layers, once the refractive indices of the layers are known. Consequently, the ATR scan of the thiopeptide–lipid monolayer in buffer solution, having the expected high angle of exciting surface plasmons ($\theta = 56°$), is shifted to still higher values, when a lipid bilayer is formed on top of the monolayer, as shown in Figure 7, while the refractive index of the lipid is supposed to remain unchanged ($n = 1.5$). The thickness increment can thus be calculated according to a multilayer model with Fresnel's formalism and optical parameters as summarized in Table 2. The increment due to the second lipid layer is remarkably close the expectation of a further 2.5 nm. Monitoring the reflectivity at a constant angle as a function of time allows kinetic data to be obtained. With reflectivities converted into the respective thicknesses, the increase in thickness due to bilayer formation is monitored in real time. At the time $t = 0$ a suspension of liposomes was added to the thiopeptide–lipid monolayer, Figure 7. The thickness eventually attained is in good agreement with the one obtained by the ATR scan, Figure 7.

Experiments with respect to bilayer formation were generally carried out at a temperature of 30 °C. At this temperature the vesicles made from egg PC rather than the monolayer are in the fluid state (the transition temperature of DMPE is 49 °C). When the same experiments were carried out at 20 °C, no increase in layer thickness was observed, also shown in Figure 7. On replacement of the suspension of pure liposomes by a suspension of liposomes with reconstituted H^+–ATPase, the increase in thickness as a function of time becomes higher as shown in Figure 8. Thickness is observed to increase over a period of about 1 h attaining a constant value of 7 to 9 nm, somewhat depending on the proportion of the enzyme reconstituted in the vesicles as summarized in Table 2. Stationary values being hardly affected by rinsing with pure buffer solution are stable for hours and almost days. An exchange of membrane constituents appears to take place between liposomes and the pure solid supported lipid bilayer. This is seen also in Figure 9 showing the kinetic trace after the exchange with liposomes containing cholesterol or ATPase in contact with a bilayer made up from pure liposomes.

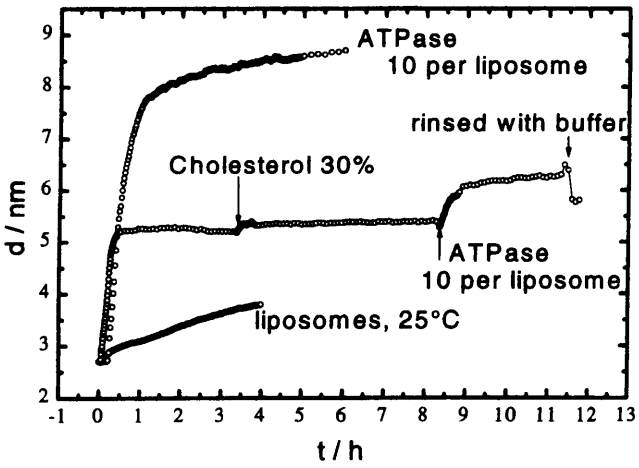

Figure 9. Real time recordings (reflectivity vs time) of the fusion of the thiopeptide–lipid monolayer with pure liposomes, after the addition of liposomes with 30% cholesterol, and after addition of liposomes containing an average of 10 ATPases per vesicle, compared with the direct fusion using the same vesicle suspension.

Discussion

The strategy of the present approach was to obtain lipid layers being attached to the support via a spacer of well-defined composition and geometrical arrangement. These layers may be seen in comparison with those having more flexible[3,4] or soft cushions of polymer spacers.[5–10] Lipid layers investigated here are made up from thiopeptide–lipid compounds which are hard to prepare in the bulk phase, while the preparation of the thiopeptides is comparatively easy. These were, therefore, attached to the gold supports by self-assembly and the covalent binding of the lipid was carried out in situ. Both processes were followed by FTIR spectroscopy. The attachment of the thiopeptide after incubation of the support is indicated by the amide, methyl, and methylene bands of the peptide. The coupling with DMPE is indicated by the methylene groups of the C_{14}-alkyl chains and the phosphate and ester functionalities occurring in the lipid rather than the peptide. More detailed information regarding structure has so far not been obtained. However, helical structures have been observed for self-assembled thiopeptides[23,24] rather than β-sheets. Therefore, thiopeptides are modeled in Figure 10 assuming a helical conformation. Theoretical dimensions are calculated from these model structures. They are used for comparison with thicknesses measured by XR and SPS, in order to derive to a model for the order and arrangement of the molecular architectures.

With respect to the thiopeptide monolayer, see Table 2, thicknesses obtained by both surface analytical methods are consistent (1.2–1.5 nm) with a roughness obtained by XR of only 0.4 nm. This corresponds to the calculated dimension of the peptide and points to a relatively smooth and complete layer with peptide molecules being arranged normal to the surface or only slightly tilted. This would be similar to arrays of long chain thioalkanes obtained by self-assembly.

Covalent attachment of DMPE also results in an increment in layer thickness (1.4–1.9 nm) consistently measured by both XR and SPS, however, too low with respect to the expectation for a lipid monolayer (2.0–2.5 nm). The reduced thickness is consistent with the increased roughness of the lipid monolayer with respect

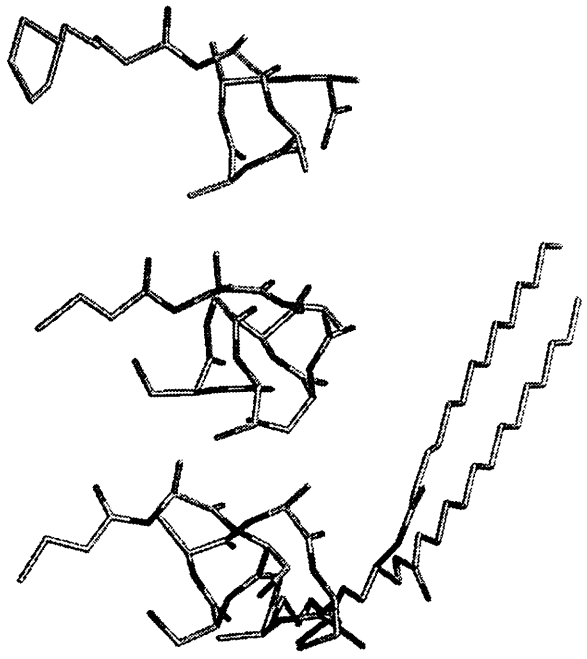

Figure 10. Molecular modeling of the thiopeptides I and II (see the Experimental Section, peptide II being used for all the experiments described in this work) and the thiopeptide–lipid construct formed in situ after chemical coupling to DMPE. The model was used to deduce the maximum length of the molecules to be 1.8, 1.6, and 4.2 nm, respectively.

to the thiopeptide found by XR. From these quantities a nearly complete coverage can be deduced for the peptide layer alone, while for the peptide–lipid not more than 70% coverage is found. Hence a perfect layer is not attained at least at the level of the lipid. This accounts for the relatively poor electric properties indicated in Table 3.

The fusion of liposomes with these imperfect monolayers appears to take place as indicated by the increase in layer thickness obtained by SPS. The thickness increment of 2.6 nm after the fusion with pure liposomes as compared to half the calculated width of a phospholipid bilayer of 2.5 nm is a strong indication that a discrete lipid bilayer is indeed obtained with not much unspecific binding of fragmented or closed vesicles. This is also in line with the observation of a clear saturation behavior in the real time recordings, Figure 7, 8, and 9, and bilayers being stable after rinsing and forming only with the lipid being in the fluid state. The relatively high value with respect to the expectation could even be a hint as to the self-healing effect on the level of the peptide-supported lipid bilayer compared to the monolayer. Incorporation of H^+–ATPase into these lipid layers had been deduced from electrochemical experiments.[14] Protons transported across the lipid membrane could be detected at the gold electrode. Currents measured due to the activity of the enzyme, however, were too high, provided the proportion of the membrane protein in the lipid layer is the same as in the liposomes. This suggests an accumulation of the enzymes in the lipid layer with respect to the liposomes. This problem is addressed in the fusion experiment with different amounts of ATPase present. The thicknesses obtained by SPS in the stationary state summarized in Table 2 do not depend considerably on the number of enzymes per liposome. An optimum is attained at the number of 10. The kinetics of the fusion process, however, appears to be slowed down with a higher amount of protein present.

The thickness obtained in all cases of confirming our earlier result of 8.5 nm,[13] however, is very high compared

(23) Lear, J. D.; Wassermann, Z. D.; DeGrado, W. D. *Science* **1988**, *240*, 1179.
(24) Enriquez, E. P.; Samuelski, E. T. *Mater. Res. Soc. Symp. Proc.* **1992**, *255*, 423.

to the expectation. The lateral dimension of the ATPase itself is 8.5 nm. That means irrespective of the the ratio of protein to lipid in the liposomes, the lipid layer appears to accumulate the ATPase. The effect is smaller, if a pure bilayer is formed prior to adding the ATPase–liposome suspension, even if the lipid bilayer contains cholesterol. Then a total thickness of only 6.5 nm is obtained as shown in Figure 9. Anyway, a certain exchange from the vesicles into the planar system appears to take place.

In conclusion, the incorporation of membrane proteins (others than the ATPase are in preparation), into the peptide supported lipid films can be monitored easily and reproducibly. This is because swelling of the aqueous layer is a minor effect in contrast to dextrane-supported lipid films.[10] The peptide spacer, on the other hand, forms a sufficiently rigid structure to allow for an "aqueous" layer 1.2 nm wide compared to 0.12 nm in the case of the poly(oxyethylene) spacer[4] and up to 10 nm in the case of dextrane.[10] Cholesterol is incorporated the same as in the dextrane-supported system.[10] It does, however, not improve the electrical properties which are poor, particularly when compared to the poly(oxyethylene)-supported sytem.[3,4] Self-healing effects appear not to make up for these deficiencies.

Acknowledgment. We are indebted to A. Offenhäusser, J. Rühe, E. Sackmann, and M. Stamm. Financial support was obtained from the Bundesministerium für Bildung, Wissenschaft, Forschung und Technologie (Fkz: 0310852), and from Merck KGaA, Darmstadt.

LA970317L